IEEE Photonics Journal
An IEEE Photonics Society Publication

Open Access

Accuracy of the Point-Source Model of a Multi-LED Array in High-Speed Visible Light Communication Channel Characterization

Volume 7, Number 4, August 2015

Jupeng Ding
Zhengyuan Xu
Lajos Hanzo, Fellow, IEEE

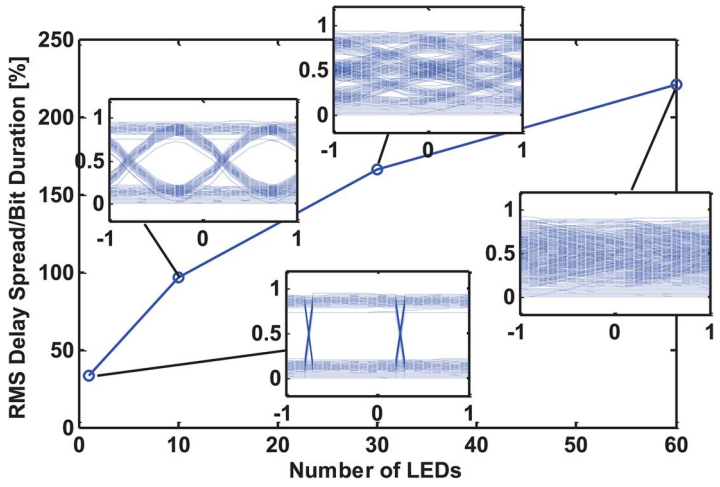

DOI: 10.1109/JPHOT.2015.2450534
1943-0655 © 2015 IEEE

IEEE photonics SOCIETY

IEEE

Accuracy of the Point-Source Model of a Multi-LED Array in High-Speed Visible Light Communication Channel Characterization

Jupeng Ding,[1] Zhengyuan Xu,[1] and Lajos Hanzo,[2] *Fellow, IEEE*

[1]Key Laboratory of Wireless-Optical Communications, Chinese Academy of Sciences, School of Information Science and Technology, University of Science and Technology of China, Hefei 230027, China
[2]School of Electronics and Computer Science, University of Southampton, Southampton SO17 1BJ, U.K.

DOI: 10.1109/JPHOT.2015.2450534

Manuscript received June 9, 2015; revised June 23, 2015; accepted June 24, 2015. Date of publication Month 00, 0000; date of current version Month 00, 0000. This work was supported in part by the National Key Basic Research Program of China under Grant 2013CB329201, by the National Natural Science Foundation of China under Grant 61171066 and Grant 61401420, and by the Shenzhen Peacock Plan under Grant 1108170036003286. Corresponding author: L. Hanzo (e-mail: lh@ecs.soton.ac.uk).

Abstract: During the indoor visible light communication (VLC) channel modeling procedure, the transmitter constituted by an array of light-emitting diodes (LED's) is frequently modeled as a single point source for convenience. However, how accurate this simplified treatment is remains unanswered. This paper compares the channel characteristics of both the simplified point-source model and six practical cases having various numbers of LEDs. Our numerical results show that the deviations in terms of the channel's optical path loss (OPL), as well as its bandwidth and the channel's delay spread, are steadily increased upon increasing the number of LEDs of each transmitter, until LEDs spread almost over the entire ceiling. Even in the worst case, the deviation of the OPL remains below 0.41 dBo, whereas that of the 3-dB transmission bandwidth is below 1. 67 MHz. However, the deviation in terms of the root-mean-square (RMS) delay spread can reach 1.88 ns. Moreover, in terms of spatial distribution of the RMS delay spread, there is a nonnegligible difference between the simplified point-source model and different transmitter configurations.

Index Terms: Visible light communication, channel characterization, modeling accuracy, point-source model.

1. Introduction

Indoor visible light communications (VLC) is capable of simultaneously realizing both data transmission and universal illumination, using white light-emitting diode (LED)-based lighting fixtures [1]–[4]. An LED lighting fixture serves as a VLC transmitter and usually consists of an array of LEDs. Numerous mature radio frequency techniques have been carefully adapted for employment in various indoor VLC systems in order to improve their performance [5]–[7]. As a critical component, the VLC channel model is expected to reliably capture the multipath propagation characteristics of the received VLC signals from the transmitter, which is frequently viewed as a

single-point source during modeling the system owing to its appealing simplicity [8], [9]. Given the limited power of each LED, which tends to be below a few hundred mW [10], [11], each LED lighting fixture has a limited coverage. Therefore, typically multiple lighting fixtures are distributed over a room's ceiling for seamless illumination coverage. Each VLC transmitter tends to be composed of a large LED array [12], [13]. This configuration is quite different from the traditional infrared medium based optical wireless communications (OWC).

As a common practice, each fixture is approximated as a point source [8], [9] regardless of the specific spatial distribution of the different LEDs within each transmitter. For example, in [8], 16 transmitters are regarded as 16 discrete point sources to verify the efficiency of the optimization scheme designed for counteracting the signal to noise ratio fluctuation. Similarly, in [14] and [15], the displacement information of all interior LEDs in each source is also disregarded. This simplification is capable of significantly reducing the modeling complexity, especially if there are hundreds of LEDs within an array [10], [11], [16]. At the time of writing, there is a paucity of studies on the accuracy of this simplification technique in the context of various VLC transmitter configurations. However, in high-speed VLC, the differences in the arrival time of rays from different LEDs may significantly affect the channel characteristics.

Hence, apart from using a point source, six different transmitter configurations corresponding to different approximation accuracies are introduced into our numerical analysis. For comparison, the LED spacing of each transmitter is set to be the same in all of the six cases. The channel characteristics are compared in terms of several metrics, including the optical path loss (OPL), the channel's useful transmission bandwidth and the root mean square (RMS) delay spread. Moreover, the spatial and statistical distributions of the aforementioned channel characteristics of all scenarios are numerically analyzed as well. Furthermore, the specific transmission performance difference of the simplified and the other actual cases is intuitively illustrated at 1 Gbps data rate. For conveniently presenting the underestimation to channel multipath dispersion under source array simplification, the on-off keying (OOK) modulation scheme is consistently adopted for all comparative cases.

The remainder of this paper is organized as follows. In Section 2, we present the mathematical description of channel characterization with and without transmitter simplification. In Section 3, we numerically analyze the influence induced by source simplification to optical path loss, 3-dB transmission bandwidth and RMS delay-spread. In the same section, the eye diagrams of 1 Gbps transmission rate are illustrated as well. Finally, Section 4 provides the conclusions.

2. Channel Characterization Both With and Without Transmitter Simplification

Current VLC schemes by definition rely on visible light as their medium of indoor wireless communication. Given their appealing simplicity, intensity modulation and direct detection (IM/DD) are widely used in VLC implementations. At the transmitter, the information bearing digital signal is firstly converted to an electronic current and then a DC current is added to ensure having a non-negative waveform. Then, the resultant signal is fed into the LED. As for the receiver, a photo-diode (PD) collects the optical intensity signal that falls in its field of view (FOV) and generates a proportional electronic current. The resultant current is then converted to a voltage with the aid of a trans-impedance amplifier (TIA). Since the VLC system is overlaid on the indoor illumination infrastructure, the distributed transmitters are composed of LED arrays in order to satisfy the illumination requirements, as shown in Fig. 1. A zoomed plot from one of the arrays in this figure clearly shows the uniformly distributed LEDs. Again, in order to reduce the complexity of multipath channel characterization, the point-source model based simplification is often adopted, where the transmitter relying on multiple LEDs is treated as an abstract point source (APS) [8], [9]. On one hand, this transmitter simplification would certainly reduce the modeling complexity. On the other hand, the time dispersion induced by the various LEDs is underestimated to some extent, since the spatial position information of each LED is discarded. Hence, the accuracy of the above simplification requires careful assessment.

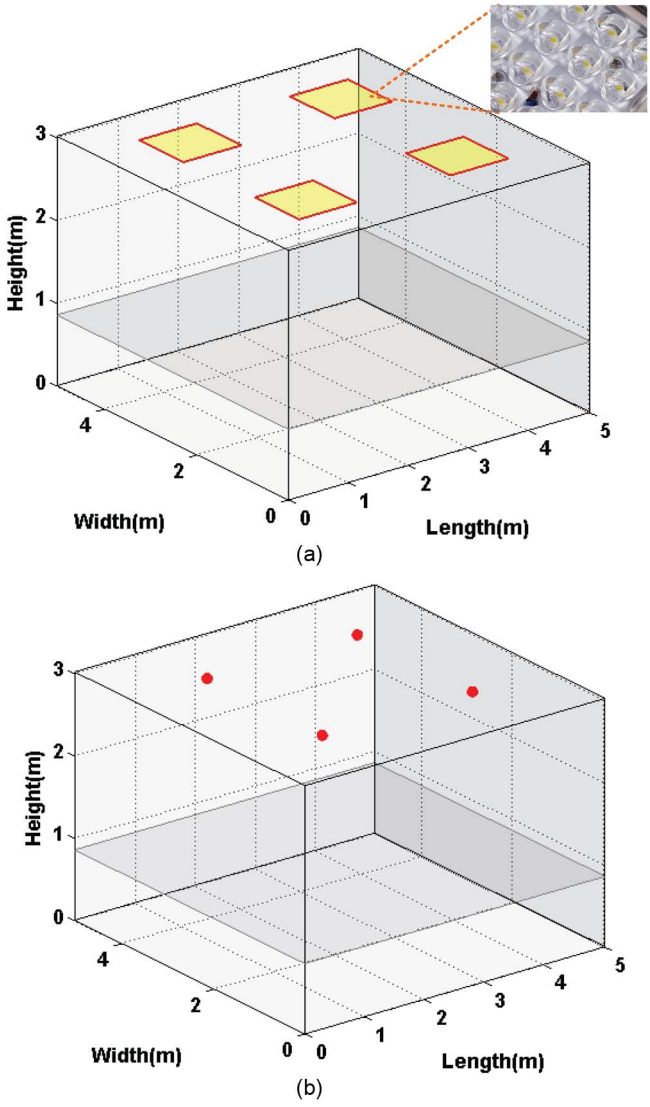

Fig. 1. View of indoor scenarios with (a) actual LED arrays and (b) simplified ones.

2.1. Scenario Without Transmitter Simplification

To evaluate the channel characteristic differences of this transmitter simplification, the VLC channel should be carefully modeled. In general, the impulse response is used for characterizing the VLC channel. Typically, there is a direct line-of-sight (LOS) path and reflected paths.

In the more accurate model dispensing with transmitter simplification, the LOS path between the source $S_{n,i}$ (the ith LED in the nth array) and the jth receiver R_j on the working plane can be characterized as [10], [11], [15]

$$h^{(0)}(t; S_{n,i}, R_j) = \begin{cases} \frac{1}{d_0^2} A_R R(\phi_0) \cos\theta_0 \delta\left(t - \frac{d_0}{c}\right), & 0 \le \theta_0 \le FOV \\ 0, & \theta_0 \ge FOV \end{cases} \quad (1)$$

where A_R is the effective receiver area, and m is the mode index of a specific radiation lobe. The distance between a source and a receiver is represented by d_0, while ϕ_0 is the irradiance angle with respect to the normal axis of the LED, and θ_0 is the incidence angle with respect to the normal axis of the receiver. The *FOV* represents the angle of reception at the receiver which is mainly

decided by the components of receiver, such as optical concentrator with optical filter. Moreover, δ is the Dirac delta function and c denotes the speed of light. Finally, $R(\phi_0)$ is the emitted power in one spatial direction.

The emission from single commercially available LED usually can be modeled by *Lambertian* radiation pattern. Under this condition, the radiant intensity in any direction can be calculated by

$$R(\phi_0) = \frac{m+1}{2\pi} P_s \cos^m \phi_0 \tag{2}$$

where P_s is the average transmitted optical power which is set 1 W in this paper for convenience of analysis, and m indicates the Lambertian index of the LED given by

$$m = -\frac{\ln(2)}{\ln\left(\cos\phi_{\frac{1}{2}}\right)} \tag{3}$$

where $\phi_{1/2}$ is the semi-angle (at half power) of the LED. Generally, $\phi_{1/2} = 60^\circ$ which corresponds to $m = 1$. *In an indoor environment, most reflections are diffuse reflections in nature and a Lambertian model can be used. Actually, the time dispersion is mainly decided by the multi-path propagation induced by reflection interaction between the emitted optical signal and the illuminated inner surface of the indoor scenario*. As the modeling algorithm is finally implemented by computer, the indoor surface must be divided into reflective elements of equal size and the central position is viewed as the coordinates of the respective reflective element. For the first order reflection, the mentioned interaction can be decomposed into two steps. In the first step, the reflective element is viewed as the abstract receiver and the optical signal reaches the element via LOS path. The impulse response at any lth element ε_l can be given by

$$h^{(0)}(t; S_{n,i}, \varepsilon_l) = \begin{cases} \frac{1}{d_{l,1}^2} A_\varepsilon R(\phi_1) \cos\theta_1 \delta\left(t - \frac{d_{l,1}}{c}\right), & 0 \le \theta_1 \le 90^\circ \\ 0, & \theta_1 \ge 90^\circ \end{cases} \tag{4}$$

where A_ε is the area of one reflective element. *The distance between a source and this reflective element is represented by* $d_{l,1}$, while ϕ_1 is the irradiance angle of optical signal, and θ_1 is the incidence angle with respect to the normal direction of the surface which contains this reflective element. Unlike the case in (1), the FOV of all reflective elements is naturally 90° since all elements is omni-directional in capturing light signal from all incident directions. In the second step, the reflective element absorbs part of captured optical signal power and simultaneously serves as the secondary source to emit the left power. Since the reflective element can be viewed as generalized Lambertian source, i.e., $m = 1$, the final impulse response contribution via this first bounce path can be given by

$$h^{(1)}(t; S_{n,i}, \varepsilon_l, R_j) = \begin{cases} h^{(0)}(t; S_{n,i}, \varepsilon_l) \otimes \rho_l \frac{1}{\pi d_2^2} A_R \cos\phi_2 \cos\theta_2 \delta\left(t - \frac{d_2}{c}\right), & 0 \le \theta_2 \le FOV \\ 0, & \theta_2 \ge FOV \end{cases} \tag{5}$$

where ρ_l is the reflectivity of the surface to which the reflective element ε_l belongs, $\otimes$ stands for convolution, and d_2 is the distance between the reflective element ε_l and the receiver R_j, while ϕ_2 is the irradiance angle of the reflected optical signal and θ_2 is the incidence angle with respect to the normal direction of the jth receiver R_j. The total impulse response caused by all first bounce paths can be described by

$$h^{(1)}(t; S_{n,i}, R_j) = \sum_{l=1}^{N} h^{(1)}(t; S_{n,i}, \varepsilon_l, R_j) \tag{6}$$

where N is the number of all reflective elements. Then, the channel impulse response (CIR) for the kth-bounce can be calculated recursively as

$$h^{(k)}(t; S_{n,i}, R_j) = \sum_{l=1}^{N} h^{(k-1)}(t; S_{n,i}, \varepsilon_l) \otimes \rho_l h^{(0)}(t; \varepsilon_l, R_j) \tag{7}$$

where $h^{(k-1)}(t; S_{n,i}, \varepsilon_l)$ denotes the impulse response from the source $S_{n,i}$ to the lth reflective element ε_l through $(k-1)$th-bounce, whose similar expression can be obtained according to (7). The specific expression of $h^{(0)}(t; \varepsilon_l, R_j)$ can be obtained according to (1).

Once the influence of multiple reflections is included, the total multipath impulse response can be written as a sum of the LOS paths and of the various reflected paths

$$h(t; R_j) = \frac{1}{N_{array} I} \sum_{n=1}^{N_{array}} \sum_{i=1}^{I} \sum_{k=0}^{K} h^{(k)}(t; S_{n,i}, R_j) \tag{8}$$

where N_{array} denotes the number of transmitter LED arrays, I is the number of LEDs in each array, and K is the maximum reflection order. It should be noted that for the convenience of comparison, the total transmitted power of all transmitters in these cases is assumed to be 1 W and the impulse response $h(t; R_j)$ must be normalized by $N_{array} I$. In this paper, the reflections are calculated up to three orders, because the contribution from each of the higher-order reflected paths is small and hence can be neglected compared to the total impulse response [10], [15].

2.2. Scenario With Transmitter Simplification

As mentioned above, in the simplified scenario, the transmitters are viewed as APS. In a Cartesian coordinate system, the APS is located in the central position of the respective array. For instance, Fig. 1 presents a typical medium-sized room of 5 m × 5 m × 3 m, where the ceiling is 3 m above the floor. Following Fig. 1(a) and (b) shows 4 (2 × 2) APSs that are uniformly spread across the ceiling, whose coordinates are (1.25, 1.25, 3.0) m, (3.75, 1.25, 3.0) m, (1.25, 3.75, 3.0) m, (3.75, 3.75, 3.0) m, respectively. In general, the mathematical model of characterizing the visible light multipath propagation phenomenon must be modified in accordance with this simplified configuration. The response of the LOS path between the nth APS S_n and the jth receiver R_j can be expressed as

$$h^{(0)}(t; S_n, R_j) = \begin{cases} \frac{I}{d_{pot0}^2} A_R R(\phi_{pot0}) \cos\theta_{pot0} \delta\left(t - \frac{d_{pot0}}{c}\right), & 0 \le \theta_{pot0} \le FOV \\ 0, & \theta_{pot0} \ge FOV \end{cases} \tag{9}$$

where the definitions of A_R, m, d_{pot0}, ϕ_{pot0}, and θ_{pot0} are consistent with or similar to those variables in (1). It shows that the radiation characteristic of APS is still viewed to follow Lambertian pattern. Since all the emitted power emanating from a transmitter is concentrated in the APS, unlike in (1), the response intensity must be multiplied by I, i.e., by the number of LEDs in the transmitter. Correspondingly, the response intensity originating from the APS to the surrounding environment of the surfaces has to be enhanced by a factor of I as well. For the first step of first order reflection, the impulse response at any lth element ε_l also must be modified to

$$h^{(0)}(t; S_n, \varepsilon_l) = \begin{cases} \frac{I}{d_{pot1}^2} A_\varepsilon R(\phi_{pot1}) \cos\theta_{pot1} \delta\left(t - \frac{d_{pot1}}{c}\right), & 0 \le \theta_{pot1} \le 90^\circ \\ 0, & \theta_{pot1} \ge 90^\circ \end{cases} \tag{10}$$

where d_{pot1} is the distance between any one APS and this reflective element, while ϕ_{pot1} is the irradiance angle of optical signal from this APS and θ_{pot1} is the incidence angle with respect to the normal direction of the concerned reflection surface. Since the step from the reflective element to the receiver is same as the counterpart of case without transmitter simplification, the final

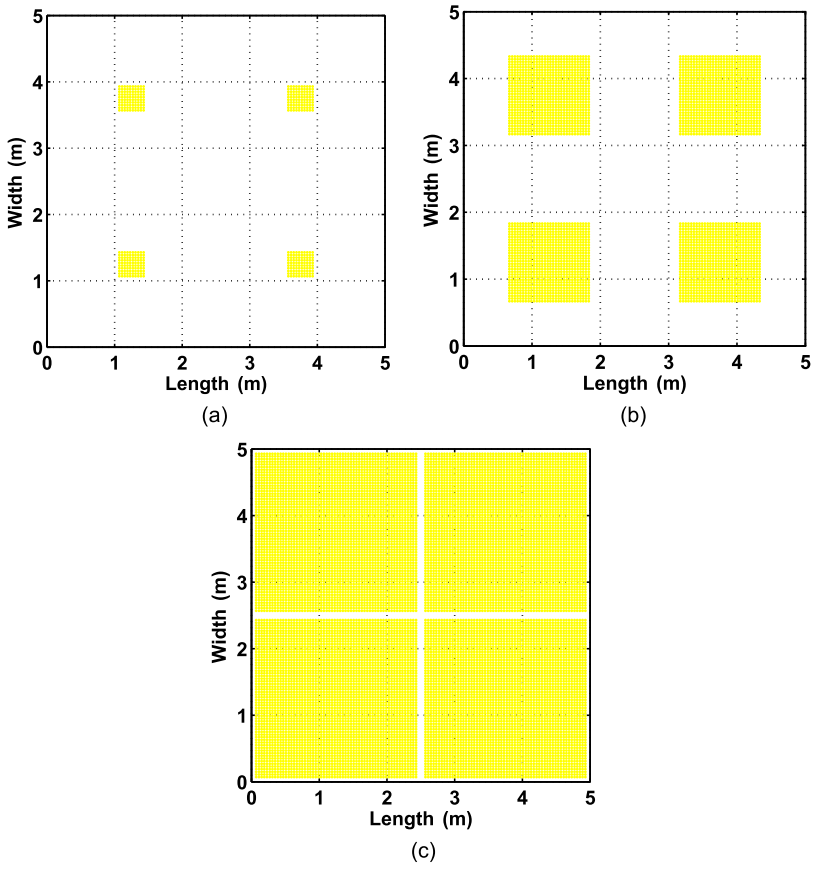

Fig. 2. Layout of the LED arrays (a) 10 × 10, (b) 30 × 30, and (c) 60 × 60.

impulse response contribution via one 1st bounce path and all 1st bounce paths can easily be derived following (5) and (6). In this situation, the CIR should be correspondingly rewritten as

$$h(t; R_j) = \frac{1}{N_{pot} I} \sum_{n=1}^{N_{pot}} \sum_{k=0}^{K} h^{(k)}(t; S_n, R_j). \tag{11}$$

Here, N_{pot} stands for the number of APSs, which is equal to N_{array}, while S_n is the nth APS. It should be noted that the sum is not performed over the index i as that in (8) due to the transmitter's simplification to a point source. For consistency with the accurate scenario operating without simplification, the coefficient $1/(N_{pot} I)$ is applied in order to normalize the emitted power. Additionally, similar mathematical expression of $h^{(k)}(t; S_n, R_j)$ can be obtained following (7).

3. Numerical Results and Discussions

In this section, the channel characteristic differences imposed by the LED array simplification are analyzed in typical indoor scenarios, as depicted in Fig. 1. Following the approach of [16], the reflectance of the ceiling, wall and floor are set to 0.8, 0.5 and 0.2, respectively. The receiver is located on a virtual working plane, *which is 0.85 m above the floor* [16]. Three different transmitter configurations are considered, as shown in Fig. 2. The difference of these configurations lies in the increasing number of LEDs, while *the spacing between the pair of LEDs within a transmitter remains a constant of 4 cm* [16]. Given that the transmitters would overlap with each other if the number of LEDs in each transmitter exceeds 60 × 60, without loss of generality, the three actual transmitter configurations are assumed to be 10 × 10, 30 × 30, and 60 × 60, respectively. *As for the last case of 60 × 60 array, it is conserved to illustrate the upper limit of*

TABLE 1
Parameters for transmission characteristics simulation

Parameters	*Value*
Indoor scenario size	5 m × 5 m × 3 m
Reflectance of ceiling	0.8
Reflectance of wall	0.5
Reflectance of floor	0.2
Impulse response time resolution	0.1 ns
Reflective element size for 1st reflection	5 cm × 5 cm
Reflective element size for 2nd reflection	16.7cm × 16.7 cm
Reflective element size for 3rd reflection	50 cm × 50 cm
Coordinates of LED arrays centers & APSs	(1.25, 1.25, 3.0) m, (3.75, 1.25, 3.0) m, (1.25, 3.75, 3.0) m, (3.75, 3.75, 3.0) m
LED spacing in one array	4 cm
Elevation of LED arrays & respective APSs	-90 deg.
Azimuth of LED arrays & respective APSs	0 deg.
Height of LED arrays & respective APSs	3 m
Detection physical area of receiver	1 cm^2
FOV of receiver	90 deg.
Elevation of receiver	90 deg.
Azimuth of receiver	0 deg.
Height of receiver	0.85 m

deviation caused by transmitter simplification in typical indoor scenario. Although the case is not as practical as the left cases, for sufficiently presenting the tendency from the simplified case to the limit case, the case of 60 × 60 is essential.

In view of the reduced influence of the higher-order reflections, for the sake of reducing the computational complexity, the spatial resolutions of the surrounding surfaces are set to 20, 6, and 2 partitions per meter for the first-, second-, and third-reflection, accordingly. For clarity, the main parameters for transmission characteristics simulation are shown in Table 1. In the following numerical simulations, three important channel characteristics are investigated, namely, the OPL, the 3 dB transmission bandwidth, and the RMS delay spread.

3.1. Optical Path Loss

A key objective of the designer of a VLC link is to achieve a high Signal to Noise Ratio (SNR) at the receiver. This is challenging, because the link SNR mainly depends on the square of the received optical power. Therefore, the average received optical power or the channel's path loss is an important parameter. The OPL is defined as the reciprocal of the channel's DC gain $H(0)$, which is represented by $-\log_{10}[H(0)]$ in unit of optical dB or dBo [17]. Moreover, the channel DC gain $H(0)$ can be expressed from the CIR by $H(0) = \int h(t)dt$ [8], [10].

In order to show the OPL differences between the accurate and the simplified scenario more intuitively, the cumulative distribution functions (CDF) of all seven scenarios are given in Fig. 3(a). It can be seen that for all scenarios, the OPL range still lies between about 55.5 and 58.5 dBo. The OPL differences among all cases are relatively small, when the CDF value is less than 0.1 or over 0.9. However, higher differences are observed, when the CDF value ranges from 0.1 to 0.9, which tends to represent the majority of the receiver's working plane. To examine the statistical characteristics over a large range, the OPL performances of all scenarios are also compared in Table 2 for the CDF values in the range spanning from 0.2 to 0.8.

For the simplified scenario, the OPL varies between 55.62 and 57.09 dBo, when the CDF value lies within 0.1 ∼ 0.9. The CDF curves match very well for the 10 × 10 case and the 30 × 30 case, which exhibit slight fluctuations. In other words, the discrepancies with respect to these two actual cases are small and the relevant numerical results are shown in Table 2. The most obvious discrepancy is observed for the 60 × 60 case. However, even in this case, the absolute OPL value deviations corresponding to 0.1 and 0.9 are as low as 0.09 and 0.22 dBo, respectively. Even for the OPL level over 55 dBo, these deviations remain quite limited.

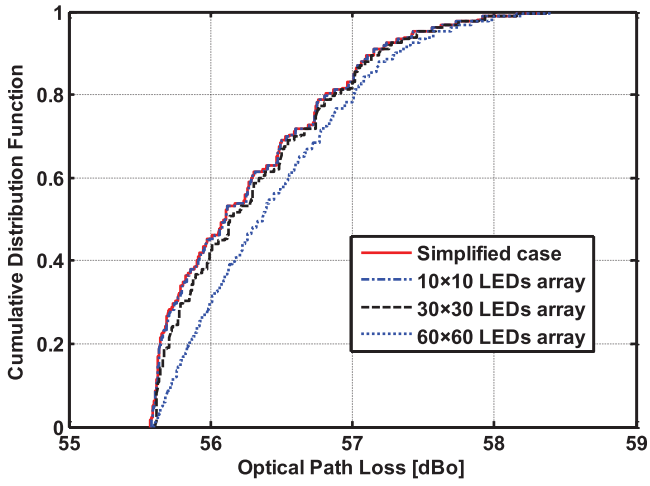

(a)

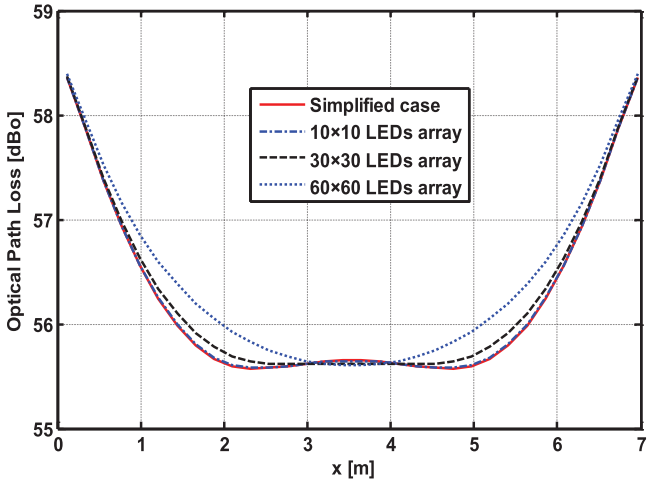

(b)

Fig. 3. (a) Cumulative distribution function and (b) cross section of OPL spatial distributions.

TABLE 2

Optical path loss variation range in the given range of CDF value

Optical path loss variation range (dBo)					
Cases with & without transmitter simplification		Transmitter simplification	Various transmitter configurations		
			10×10	30×30	60×60
CDF value range	0.1	55.62	55.62	55.63	55.71
	0.9	57.09	57.10	57.13	57.31
	0.2	55.65	55.65	55.71	55.86
	0.8	56.81	56.94	56.98	57.01

As for the CDF range between 0.2 and 0.8, the OPL varies between 55.65 and 56.81 dBo for the simplified scenario. Observe in Table 2 that the maximum deviation is still recorded for the 60 × 60 case. As seen in Fig. 3, the difference is about 0.21 and 0.20 dBo for the upper and lower limits of the OPL variation range, which are negligible compared to the OPL itself. To evaluate the spatial differences more explicitly, the OPL investigation is analyzed along the diagonal direction across the working plane. Given that the room is symmetrical, this provides us adequate OPL spatial distribution information, since this is the longest one amongst all the

cross-section candidates. As shown in Fig. 3(b), the OPL cross-section curves match well for all cases, when the receiver position is close either to the room's center or to the room's edge. The highest deviations appear at about 1.8 m separation from the room's center. Although the absolute deviation is increased upon increasing the number of LEDs in a transmitter, the maximum deviation remains as low as 0.41 dBo for the 60 × 60 LED scenario. Based upon the above evaluation, the LED array simplification can be judiciously applied in the OPL analysis, even when the LEDs cover almost the entire ceiling.

3.2. 3-dB Transmission Bandwidth

As mentioned earlier, the temporal spreading engendered by multipath propagation can be described by the CIR $h(t)$, which characterizes the channel in the time domain. On the other hand, the frequency response $H(f)$ characterizes the channel as a function of frequency

$$H(f) = \int_{-\infty}^{\infty} h(t) e^{-j2\pi ft} dt \tag{12}$$

which is the Fourier transform of the CIR $h(t)$. Note that the frequency response of the dispersive VLC channel exhibits a low pass characteristic in the electronic domain. Naturally, the VLC channel's achievable transmission bandwidth constitutes an important metric of the transmission potential.

In practice, the 3-dB channel cut-off frequency $f_{-3\,\mathrm{dB}}$ is expressed as

$$|H(f_{-3\,\mathrm{dB}})|^2 = 0.5|H(0)|^2. \tag{13}$$

Usually, the 3-dB transmission bandwidth is analyzed at typical receiver locations. In order to analyze the achievable performance over the receiver plane, the CDF of the 3-dB bandwidth's spatial distribution is given in Fig. 4(a). It can be seen that the discrepancies between the simplified case and the first two accurate practical cases remain indistinguishable in this figure, but for the 60 × 60 case (blue dashed curve), the discrepancies become relatively significant and have a tendency to increase upon increasing the transmission bandwidth.

Furthermore, our numerical results show that in the CDF range spanning from 0.1 to 0.9, the corresponding 3-dB bandwidth varies between 19.53 MHz and 21.67 MHz for the simplified scenario. For convenience of comparison, the results of all cases are summarized in Table 3. It is observed that the deviations are small for the 10 × 10 to 30 × 30 scenarios. As for the 60 × 60 case, 0.31 MHz and 1.22 MHz deviations are imposed by the array simplification on the respective lower and upper limits of the 3-dB bandwidth. Additionally, when the CDF value lies between 0.2 and 0.8, the 3-dB bandwidth changes from about 19.84 MHz to 21.21 MHz, which implies a difference of 1.37 MHz for the simplified scenario, which is increased to 1.83 MHz associated with a 3-dB bandwidth change from 20.14 MHz to 21.97 MHz for the case of 60 × 60, as seen in Table 3. The deviation from the actual bandwidth remains less than 5%,which is acceptable for practical engineering applications.

The relevant cross-sections along the diagonal direction are characterized in Fig. 4(b). A pronounced received signal peak can be observed at the room's center. Given that the locations of all the four point sources are symmetrically arranged to the room's center, the optical signals arriving via the LOS paths arrive at the receiver simultaneously. As a result, the multipath effects engendered by the presence of multiple sources remain modest at this location and hence a high bandwidth can be obtained. Moreover, when moving from the 10 × 10 case to the 60 × 60 case, the peak bandwidth increases. More particularly, in the 60 × 60 case, the 3-dB bandwidth more smoothly changes near the room's center. At the same time, owing to the reflections from the wall, the 3-dB bandwidth varies drastically with the receiver locations, especially near the corner of the room. Similar phenomena can be observed for the simplified scenario.

Specifically, the multipath effects induced by the multiple transmitters become more severe, as the distance between the receiver and the room's center increases. The bandwidth decays

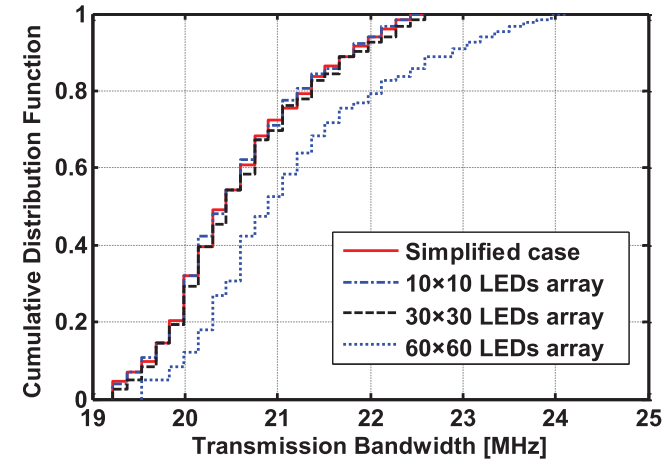

(a)

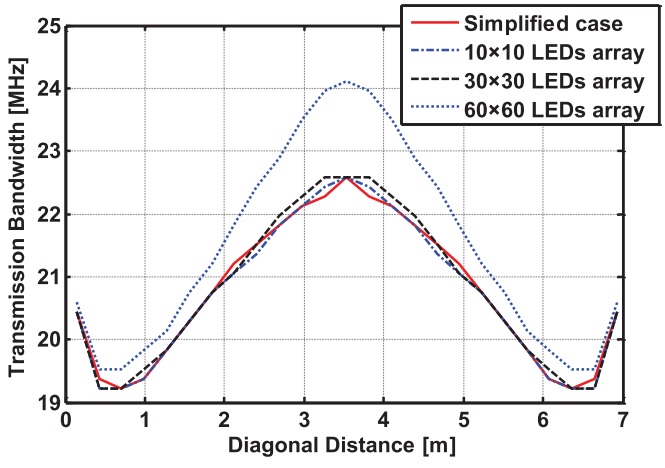

(b)

Fig. 4. (a) CDF and (b) cross section of transmission bandwidth spatial distributions.

TABLE 3

Three-decibel transmission bandwidth variation range in the given range of CDF value

3-dB transmission bandwidth variation range (MHz)					
Cases with & without transmitter simplification		Transmitter simplification	Various transmitter configurations		
			10×10	30×30	60×60
CDF value range	0.1	19.53	19.53	19.53	19.84
	0.9	21.67	21.67	21.82	22.89
	0.2	19.84	19.84	19.84	20.14
	0.8	21.21	21.21	21.21	21.97

smoothly towards its minimum at the positions close to the edge of the room. Upon further increasing the distance, however, in the extreme vicinity of the room's perimeter, the bandwidth increases again due to the reflection of the VLC components from the wall, since these reflected components become more dominant. Observe in Fig. 4 that the bandwidth differences between the 10 × 10 case and the 30 × 30 case are less than 0.7 MHz. However, for the 60 × 60 case, we observe that the associated bandwidth differences change more drastically along the diagonal and the most remarkable difference is observed near the center. Numerically, the maximum bandwidth difference imposed by the point-source array simplification is about 1.67 MHz, which accounts for about 7% of the respective actual 3-dB bandwidth.

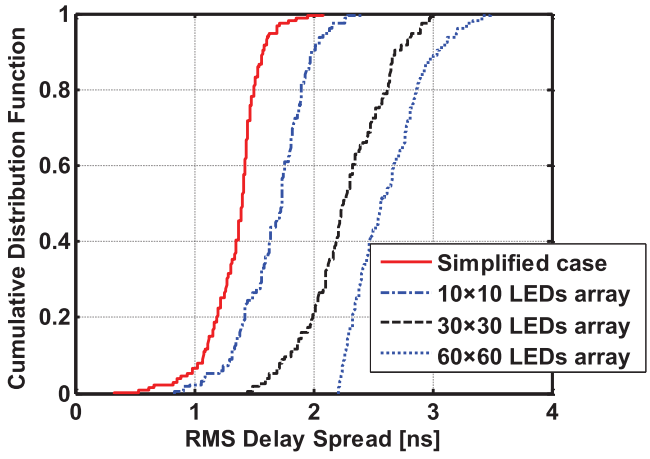

(a)

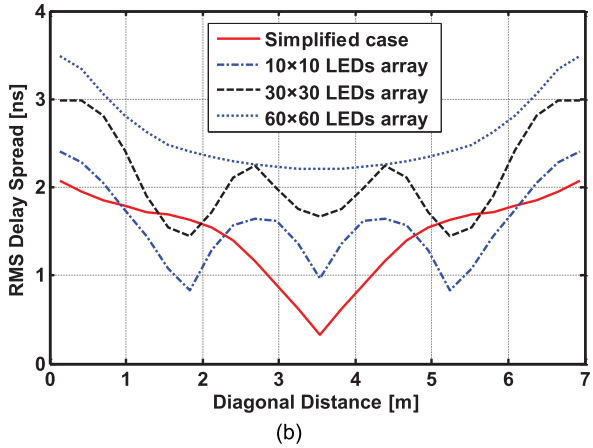

(b)

Fig. 5. (a) CDF and (b) cross section of RMS delay spread spatial distributions.

3.3. Channel's Delay Spread

Another important measure used for quantifying the temporal dispersion of wireless channels is the RMS delay-spread, which can be calculated from the CIR by [15]

$$\tau_{RMS} = \sqrt{\frac{\int_{-\infty}^{\infty} (t-\tau_0)^2 h^2(t)dt}{\int_{-\infty}^{\infty} h^2(t)dt}} \tag{14}$$

where τ_0 is the mean delay given by

$$\tau_0 = \frac{\int_{-\infty}^{\infty} t h^2(t)dt}{\int_{-\infty}^{\infty} h^2(t)dt}. \tag{15}$$

Let us now compare the spatial distribution of the RMS delay-spread in terms of the relevant CDF curves in Fig. 5(a).

Compared to the simplified case, an observable average delay-spread shift of about 0.32 ns appears for the 10 $\times$ 10 case. When the number of LEDs in each transmitter increases from 10 $\times$ 10 to 60 $\times$ 60, the delay-spread observed at a CDF value of 0.5 further increases from

TABLE 4

RMS delay-spread variation range in the given range of CDF value

RMS delay-spread variation range (ns)					
Cases with & without transmitter simplification		Transmitter simplification	Various transmitter configurations		
			10×10	30×30	60×60
CDF value range	0.1	1.08	1.32	1.81	2.27
	0.9	1.58	1.98	2.69	3.04
	0.2	1.18	1.42	2.00	2.33
	0.8	1.51	1.90	2.61	2.86

about 1.73 ns to about 2.562 ns. When the CDF values are in the range spanning from 0.1 to 0.9, the delay-spread values are listed in Table 4, which vary between 1.08 ns and 1.58 ns for the simplified case. As expected, the largest delay-spread range is observed in Table 3 for the 6060 case, which ranges from 2.27 ns to 3.04 ns. This phenomenon is largely due to the significant optical signal dispersion induced by increasing the number of LEDs, which are placed further apart.

Apart from the above statistical analysis of the RMS delay-spread, the associated differences are also illustrated in the spatial dimension along the room's diagonal, as shown in Fig. 5(b). Upon increasing the number of LED arrays, the depth of the central groove of the delay-spread plot decreases gradually. Upon moving from the 10 × 10 to the 30 × 30 case, another two grooves can be observed at positions exactly under the two arrays, which appear in the diagonal direction. In the 60 × 60 case, all grooves vanish and the RMS delay spread changes smoothly over the entire plane, albeit it remains above 2 ns. Therefore, the array simplification causes significant inaccuracy in the associated delay-spread estimation.

3.4. Eye Diagrams of High Speed Transmission

To intuitively illustrate the multipath dispersion effects under various transmitter modeling on communication system performance, consider the channel model for a baseband OOK system with non-return-to-zero (NRZ) pulse scheme. To clearly reveal the effects induced by various dispersion channel conditions, the optical sources and receivers are viewed as ideal in transmission capability. Up to now, many reported VLC systems can provide more than several hundreds Mbps, even up about 3 Gbps level [18]–[20]. However, almost all of them are implemented under stringently directed LOS channel configuration. For successful commercial application in the near future, the VLC access technique must enhance its robustness and user friendliness under non-directed multipath dispersion channel configuration in actual indoor scenarios. The transmitted data rate is set as 1 Gbps and the receiver is located at the center of working plane, i.e., (2.5, 2.5, 0.85) m for minimizing the potential channel multipath dispersion. The received signal eye diagram for discussed four cases is shown in Fig. 6. It is intuitive to see that the eyes are almost totally open in the case with transmitter simplification as the minimal signal distortion induced by the multipath dispersion channel. The respective RMS delay spread to bit duration ratio is just 32.9% which is the minimum of all concerned four cases as well. On the other side, in three cases without transmitters simplification, the induced signal waveform distortion is obviously severer than the cases with transmitters simplification. The severity continuously is deepened with the increasing number of LEDs in one transmitter. In the 10 × 10 case corresponding to 10 LED per row in Fig. 6, the eye is open to a large extent. As for the 30 × 30 case corresponding to 30 LED per row, the respective eyes diagram is distorted significantly while the RMS delay spread to bit duration ratio is impressively as large as 166.3%. In the left limit case, i.e., when the LEDs almost cover the whole ceiling, this ratio is finally up to unacceptable 220.6%. The eyes are completely closed by multipath distortion in the 60 × 60 case. Above results verify that under high speed transmission situation, the transmitter simplification can underestimate the signal waveform distortion induced by multipath dispersion channel. Such underestimation is unaffordable for cases with transmitters of relatively large size.

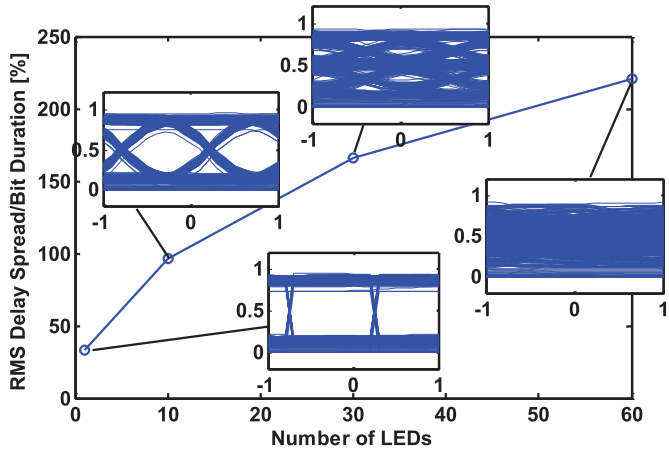

Fig. 6. RMS delay spread to bit duration ratio versus number of LEDs with eye diagrams marked.

4. Conclusion

The accuracy of the point-source transmitter simplification of the VLC channel characterization was analyzed in terms of the OPL, the 3-dB transmission bandwidth, and the RMS delay-spread. According to the numerical results, the OPL deviations are less than 0.5 dBo for all cases. As for the transmission bandwidth, the highest deviations remain below 7% for the transmitter configuration of 60 $\times$ 60 LEDs. However, significant discrepancies are observed in terms of the RMS delay-spread, since the deviation may reach 40% in the worst case. The deviations are acceptable only when the LED array size is moderate. In conclusion, the often-used transmitter simplification of concentrating all LEDs into a single point-source causes large delay-spread errors.

Acknowledgements

The authors would like to thank K. Wang for supporting them.

References

[1] J. Y. Sung, C. W. Chow, and C. H. Yeh, "Dimming-discrete-multi-tone (DMT) for simultaneous color control and high speed visible light communication," *Opt. Exp.*, vol. 22, no. 7, pp. 7538–7543, Mar. 2014.
[2] J. Gancarz, H. Elgala, and T. D. C. Little, "Impact of lighting requirement on VLC systems," *IEEE Commun. Mag.*, vol. 51, no. 12, pp. 34–41, Dec. 2013.
[3] J. Jiang, R. Zhang, and L. Hanzo, "Analysis and design of three-stage concatenated colour-shift keying," *IEEE Trans. Veh. Technol.*, to be published. AQ1
[4] X. Bao, X. Zhu, T. Song, and Y. Ou, "Protocol design and capacity analysis in hybrid network of visible light communication and OFDMA systems," *IEEE Trans. Veh. Technol.*, vol. 63, no. 4, pp. 1770–1778, May 2014.
[5] R.-H. Horng *et al.*, "Compressive sensing-based channel bandwidth improvement in optical wireless orthogonal frequency division multiplexing link using visible light emitting diode," *Opt. Exp.*, vol. 22, no. 17, pp. 19 990–19 999, Aug. 2014.
[6] C.-H. Yeh, Y.-L. Liu, and C.-W. Chow, "Real-time white-light phosphor-LED visible light communication (VLC) with compact size," *Opt. Exp.*, vol. 21, no. 22, pp. 26 192–26 197, Oct. 2013.
[7] C. H. Yeh, C. W. Chow, H. Y. Chen, J. Chen, and Y. L. Liu, "Adaptive 84.44–190 Mbit/s phosphor-LED wireless communication utilizing no blue filter at practical transmission distance," *Opt. Exp.*, vol. 22, no. 8, pp. 9783–9788, Apr. 2014.
[8] Z. Wang, C. Yu, W. D. Zhong, J. Chen, and W. Chen, "Performance of a novel LED lamp arrangement to reduce SNR fluctuation for multi-user visible light communication systems," *Opt. Exp.*, vol. 20, no. 4, pp. 4564–4573, Feb. 2012.
[9] Z. Wang, C. Yu, W. D. Zhong, and J. Chen, "Performance improvement by tilting receiver plane in MQAM OFDM visible light communications," *Opt. Exp.*, vol. 19, no. 14, pp. 13 418–13 427, Jun. 2011.
[10] J. Ding, Z. Huang, and Y. Ji, "Evolutionary algorithm based uniform received power and illumination rendering for indoor visible light communication," *J. Opt. Soc. Amer. A, Opt. Image Sci.*, vol. 29, no. 6, pp. 971–979, May 2012.
[11] T. Komine and M. Nakagawa, "Fundamental analysis for visible-light communication system using LED lights," *IEEE Trans. Consum. Electron.*, vol. 50, no. 1, pp. 100–197, Feb. 2004.

[12] J. Ding and Y. Ji, "Evolutionary algorithm based optimization of the SNR for indoor visible light communication utilizing white LED," *IET Optoelectron.*, vol. 6, no. 6, pp. 307–317, Dec. 2012.
[13] J. Grubor, S. Randel, K. D. Langer, and J. W. Walewski, "Broadband information broadcasting using LED-based interior lighting," *IEEE J. Lightw. Technol.*, vol. 26, no. 24, pp. 3883–3892, Feb. 2008.
[14] D. Wu, Z. Ghassemlooy, S. Rajbhandari, H. L. Minh, and A. C. Boucouvalas, "Improvement of the transmission bandwidth for indoor optical wireless communication systems using an elliptical Lambertian beam," *IEEE Photon. Technol. Lett.*, vol. 25, no. 2, pp. 107–110, Nov. 2013.
[15] K. Lee, H. Park, and J. Barry, "Indoor channel characteristics for visible light communications," *IEEE Commun. Lett.*, vol. 15, no. 2, pp. 217–219, Nov. 2011.
[16] T. Komine, J. H. Lee, S. Haruyama, and M. Nakagawa, "Adaptive equalization system for visible light wireless communication utilizing multiple white LED lighting equipment," *IEEE Trans. Wireless Commun.*, vol. 8, no. 6, pp. 2892–2900, Jun. 2009.
[17] M. R. Pakravan, M. Kavehrad, and H. Hashemi, "Indoor wireless infrared channel characterization by measurements," *IEEE Trans. Veh. Technol.*, vol. 50, no. 4, pp. 1053–1073, Jun. 2001.
[18] G. Cossu, A. M. Khalid, P. Choudhury, R. Corsini, and E. Ciaramella, "3.4 Gbit/s visible optical wireless transmission based on RGB LED," *Opt. Exp.*, vol. 20, no. 26, pp. B501–B506, Dec. 2012.
[19] H. Li, X. Chen, J. Guo, and H. Chen, "A 550 Mbit/s real-time visible light communication system based on phosphorescent white light LED for practical high-speed low-complexity application," *Opt. Exp.*, vol. 22, no. 22, pp. 27 203–27 213, Nov. 2014.
[20] Y. Wang, N. Chi, Y. Wang, L. Tao, and J. Shi, "Network architecture of a high-speed visible light communication local area network," *IEEE Photon. Technol. Lett.*, vol. 27, no. 2, pp. 197–200, Jan. 2015.

AUTHOR QUERY

AUTHOR PLEASE ANSWER QUERY

AQ1 = Please provide publication update in Ref. [3].

END OF QUERY